



OLCI Level 2

Algorithm Theoretical Basis Document

Instrumental Corrections

DOCUMENT REF: S3-L2-SD-03-C04-ACR-ATBD
DELIVERABLE REF: SD-03-C

VERSION: 1.2



Document Signature Table

| | Name | Function | Company | Signature | Date |
|-----------------|-------------------------|------------------------|---------|-----------|------|
| Prepared | E. Vincent I. Muguet | OLCI Technical team | ACRI-ST | | |
| Approved | L. Bourg | OLCI expert | ACRI-ST | | |
| Released | O. Fanton d'Andon | OLCI coordinator | ACRI-ST | | |

Change record

| Issue | Date | Description | Change pages |
|-------|------------|-----------------|----------------------|
| 1.0 | 06/04/2009 | Initial version | |
| 1.2 | 09/04/2010 | CDR version | 10, 13, 14, 22 to 26 |
| | | | |

Distribution List

| Organisation | To | Nb. of copies |
|-----------------|-----------------------------|------------------|
| ESA | P. Goryl | |
| EUMETSAT | Hilary Wilson, Anne OCarrol | |
| S3 Optical team | All OLCI team | |



Table of content

| | |
|--|-----------|
| 1. INTRODUCTION..... | 6 |
| 1.1 PURPOSE AND SCOPE | 6 |
| 1.2 ACRONYMS..... | 7 |
| 2. ALGORITHM OVERVIEW | 8 |
| 2.1 OBJECTIVES..... | 8 |
| 2.2 OLCI SPECTRAL CHARACTERISTICS | 8 |
| 2.2.1 Expected OLCI in-FOV spectral variation..... | 10 |
| 2.2.2 The MERIS example..... | 10 |
| 3. ALGORITHM DESCRIPTION | 16 |
| 3.1 THEORETICAL DESCRIPTION..... | 17 |
| 3.1.1 The radiance to reflectance conversion..... | 17 |
| 3.1.2 The reflectance correction..... | 18 |
| 3.2 ALGORITHM VALIDATION | 22 |
| 3.3 PRACTICAL CONSIDERATION | 22 |
| 4. ASSUMPTIONS AND LIMITATIONS..... | 23 |
| 5. AUXILIARY DATA | 24 |
| 6. ERROR BUDGET..... | 25 |
| 7. REFERENCES | 26 |



List of Figures

Figure 1: The CCD array. The pixel spatial resolution on ground is 260m..... 8

Figure 2: Top: Examples of in-flight spectral characterisation data highlighting the “smile effect”. Bottom: Spectral shift within the FOV of camera #3 according to characterisation data at several detector rows spread over the whole spectral domain..... 11

Figure 3: The “smile effect” at camera borders..... 12

Figure 4: examples of in-FOV variation of wavelength for MERIS at 442, 665, 761 and 865 nm from top to bottom. Variations are white (independent of channel average wavelength) and reaches 1.7 nm peak to peak, and up to 1 nm within a given camera (from 0.4% and 0.25% resp. at 412 to 0.2% and 0.12% resp. at 865nm). 13

Figure 5: examples of in-FOV variation of in-band irradiance for MERIS at 442, 665, 761 and 865 nm from top to bottom. Variations can go from fairly stable (0.5% at 665nm) up to really significant (2.1% at 442)..... 14

Figure 6: examples of MERIS bands normalised Spectral Response curves for typical (10 and 7.5 nm, top left and right) and extremes (3.75 and 20 nm, bottom left and right) bandwidths. Curves are given at camera FOV centre, and intra-camera spectral shift shall be added on top. 15

Figure 7: Logarithm of the Rayleigh reflectance at $\theta_s = 30^\circ$, $\theta_v = 18.5^\circ$, $\Delta\phi = 135^\circ$, $w = 5\text{m/s}$, as a function of wavelength. 19

Figure 8: Derivatives of the Rayleigh reflectance computed with the Rayleigh reflectance versus the logarithm of the Rayleigh reflectance..... 20

Figure 9: Mediterranean scene used to test the smile algorithms. The transect used for Figure 10 is East to West, north of Corsica..... 21

Figure 10: ratio of smile-corrected over non-corrected TOA reflectance in band 1 along a transect in the image in Figure 9..... 21



**SENTINEL-3 OPTICAL PRODUCTS AND ALGORITHM
DEFINITION**

**OLCI Level 2 Algorithm Theoretical Basis Document
Instrumental Corrections**

Ref: S3-L2-SD-03-C04-ACR-ATBD
Issue 1.2
Date: 2010-04-09
Page 5 of 26

List of Tables

| | |
|---|----|
| Table 1: OLCI band settings. | 9 |
| Table 2: Standard configuration of the reflectance correction. | 17 |



1. INTRODUCTION

1.1 Purpose and scope

OLCI is an imaging spectrometer which will be on-board Sentinel 3 satellite. It's the successor of MERIS, which is presently on-orbit aboard Envisat satellite. Therefore, it inherits the major part of its technical features: it operates in the reflective solar spectral range (390 nm to 1040 nm) with twenty-one (instead of fifteen for MERIS) spectral bands. The instrument has a field of view of 68.5° and covers a swath width of 1250 km. The field of view is shared between five identical optical modules arranged in a fan-shape configuration. The instrument images the Earth's surface using a 'push broom' method. For each imaging line the signal is dispersed to illuminate a 2-D CCD array, on which one direction represents the across-track direction (i.e. along an image line) and the other one the spectral dimension. The 21 spectral bands, that are programmable by ground command both in width and in position by steps of 1.25nm, are constructed by first binning spectral samples directly on the array into micro-bands, and further grouping them digitally into bands before transmission to ground.

Despite the fact that the 5 optical modules have a strictly identical design, limitations in the manufacturing procedures imply slight differences between the modules characteristics. In particular, one can expect that the spectrometers' dispersion laws slightly differ from module to module and thus induce camera to camera variations of the spectral channels central wavelength. In addition, if a row on the detector array should ideally correspond to a constant wavelength across the module's field-of-view, actual characteristics of the optics and slight misalignments of the sub-systems generally induce small variations, often referred to as the "smile effect".

This document aims at providing a comprehensive description of the instrument's spectral characteristics and their potential impact on algorithms likely to expect data acquired at a constant wavelength. It describes an algorithm that (a) properly accounts for the instrument spectral characterisation to convert TOA radiances into TOA reflectances and (b) provides a first order correction of the TOA reflectance for the wavelength variation, accounting for the surface underneath.



**SENTINEL-3 OPTICAL PRODUCTS AND ALGORITHM
DEFINITION**

**OLCI Level 2 Algorithm Theoretical Basis Document
Instrumental Corrections**

Ref: S3-L2-SD-03-C04-ACR-ATBD
Issue 1.2
Date: 2010-04-09
Page 7 of 26

1.2 Acronyms

| | |
|-------|--|
| CCD | Charge Coupled Device |
| ESA | European Space Agency |
| FOV | Field-of-view |
| FWHM | Full width at half modulation |
| LUT | Look-up table |
| MERIS | MEdium Resolution Imaging Spectrometer |
| N/A | Not Available |
| OGVI | OLCI Global Vegetation Index |
| OTCI | OLCI Terrestrial Chlorophyll Index |
| TBC | To Be Confirmed |
| TBD | To Be Defined |
| TSM | Total Suspended Matter |
| OLCI | Ocean and Land Colour Instrument |
| TOA | Top of Atmosphere |

2. ALGORITHM OVERVIEW

2.1 Objectives

The objectives of the algorithms described herein are to provide a mean to downstream algorithms to exploit OLCI data with best possible performance, accounting for the specificities of a multi-detector instrument, and in particular of the in-FOV variations of its spectral characteristics: channel central wavelengths and width.

2.2 OLCI spectral characteristics

OLCI is an imaging spectrometer that will be taken on board Sentinel 3 satellite (European Space Agency mission in the frame of GMES initiative). It is mainly devoted to the ocean and land colour remote sensing and measures the solar radiation reflected by the Earth in 21 spectral bands, programmable in width and position, in the visible and near infra-red.

OLCI is composed of 5 cameras and measures the reflected sunlight using CCD technique; indeed each camera is equipped with a spectrometer and a two-dimensional CCD array located at the optics focal plane. The picture below illustrates the CCD sensor: each CCD horizontal line provides an image line of the swath covered by one camera; the other dimension provides the spectrally dispersed radiance for each pixel along the image line, with a spectral sampling of 1.25 nm.

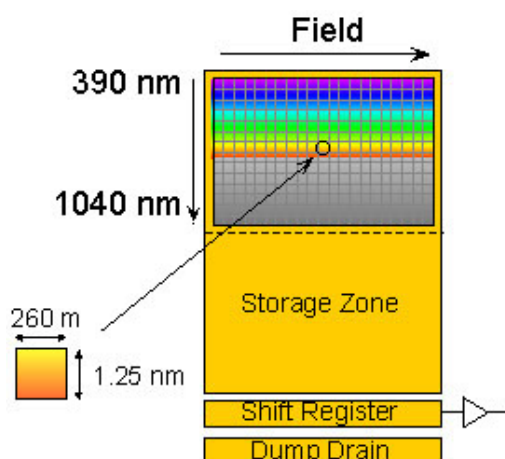


Figure 1: The CCD array. The pixel spatial resolution on ground is 260m.

The spectral measurements of each pixel along an image line are made by its own set of CCD cells: this induces small variations of the spectral wavelength of each pixel along the image that constitute the so-called "smile effect".



In the case of MERIS, the variation of the wavelength per pixel can reach 1.7 nm from one camera to another and 1.0 nm within one camera.

Even though these variations are small compared to the spectral bandwidth of a band, which is typically 10nm, and can hardly be seen in a radiance image, they can cause disturbances in Level 2 processing algorithms expecting constant wavelengths, because they either observe spectrally sensitive quantities (e.g. oxygen transmittance around 761, chlorophyll fluorescence, vegetation red edge, ...), or make use of spectrally sensitive auxiliary data at fixed wavelengths (e.g. the Rayleigh reflectance for atmosphere corrections). These disturbances can result in a visual artefact, "camera borders", or in a reduced accuracy of the Level 2 products.

The following table shows the current definition of the OLCI bands.

Table 1: OLCI band settings.

| Band | first spectral element | number of spectral elements | central wavelength | start wavelength | stop wavelength | spectral width |
|-------------|------------------------|-----------------------------|--------------------|------------------|-----------------|----------------|
| | (detectors) | | (nm) | | | |
| OA1 | 3 | 12 | 400 | 392,5 | 407,5 | 15 |
| OA2 | 15 | 8 | 412,5 | 407,5 | 417,5 | 10 |
| OA3 | 39 | 8 | 442,5 | 437,5 | 447,5 | 10 |
| OA4 | 77 | 8 | 490 | 485 | 495 | 10 |
| OA5 | 93 | 8 | 510 | 505 | 515 | 10 |
| OA6 | 133 | 8 | 560 | 555 | 565 | 10 |
| OA7 | 181 | 8 | 620 | 615 | 625 | 10 |
| OA8 | 217 | 8 | 665 | 660 | 670 | 10 |
| OA9 | 225 | 6 | 673,75 | 670 | 677,5 | 7,5 |
| OA10 | 231 | 6 | 681,25 | 677,5 | 685 | 7,5 |
| OA11 | 252 | 8 | 708,75 | 703,75 | 713,75 | 10 |
| OA12 | 289 | 6 | 753,75 | 750 | 757,5 | 7,5 |
| OA13 | 297 | 2 | 761,25 | 760 | 762,5 | 2,5 |
| OA14 | 299 | 3 | 764,375 | 762,5 | 766,25 | 3,75 |
| OA15 | 302 | 2 | 767,5 | 766,25 | 768,75 | 2,5 |
| OA16 | 306 | 12 | 778,75 | 771,25 | 786,25 | 15 |
| OA17 | 373 | 16 | 865 | 855 | 875 | 20 |
| OA18 | 393 | 8 | 885 | 880 | 890 | 10 |
| OA19 | 405 | 8 | 900 | 895 | 905 | 10 |
| OA20 | 433 | 16 | 940 | 930 | 950 | 20 |
| OA21 | 489 | 32 | 1020 | 1000 | 1040 | 40 |



2.2.1 Expected OLCI in-FOV spectral variation

OLCI spectral characterisation is obviously not yet available and the evaluation of the spectral variations to be expected across its field of view can only rely on OLCI specifications and MERIS experience.

The OLCI specifications regarding channels definition, in addition and with respect to the values of Table 1, are:

| | |
|------------|--|
| OL-DE-020: | The spectral misregistration shall be less than 1.4 nm (goal: 1 nm) |
| OL-IQ-100: | The position of the solar channels centre shall not vary by more than 1.0 nm (goal: 0.2 nm) RMS. |

Where the spectral misregistration is defined as “the maximum difference between the spectral channel central wavelengths of all the samples acquired in a given channel over an image”.

In clear that can be translated as: OLCI channels central wavelength can vary by up to 1.4 nm within the field-of-view but the overall RMS difference with respect to specified value shall remain below 1nm.

A lot of different situations can comply with such a specification, and that makes difficult to evaluate the kind of impact that can be expected. However, considering the instrument design, a few reasonable assumptions can be drawn:

1. overall tilt of the iso-wavelength line wrt the CCD array rows within a given camera (alignment)
2. curvature of the iso-wavelength line wrt the CCD array rows within a given camera (optical distortion, chromatism ; this is what is in general called “smile”)
3. discontinuities of the spectral dispersion law between cameras (manufacturing limited accuracy)

According to communication from ESA, the OL-IQ-100 requirement is meant to address temporal variation rather than in-FOV variations. This clarification puts even less constraint on the OLCI spectral homogeneity performance but does not significantly change the overall figure. The only remaining fact is that there should not be intra- or inter-camera variations higher than 1.4 nm. Since the cameras of OLCI can be programmed independently from each other, channel per channel, with a step of 1.25 nm, we remain with the following assumption:

- ❖ spectral discontinuities at camera interfaces shall be less than 1.4 nm,
- ❖ spectral variation inside any camera shall be less than 1.4 nm

The first assumption is not met by MERIS, the second one is below the MERIS performance.

It is thus reasonable to consider the MERIS case as an attempt to quantify the problem.

2.2.2 The MERIS example

Due to late problem discovery, the MERIS instrument had to be dismantled and re-assembled after a maintenance process. On-ground spectral characterisation obtained before this intervention was not fully relevant anymore and was measured again, but to a

lesser extent. The set of characterisation points was not judged sufficient to derive a reliable global spectral model of the instrument and a set of in-flight methods were designed and operated (see [1] or [2]).

The examples below show the smile effect as it was characterised on MERIS.

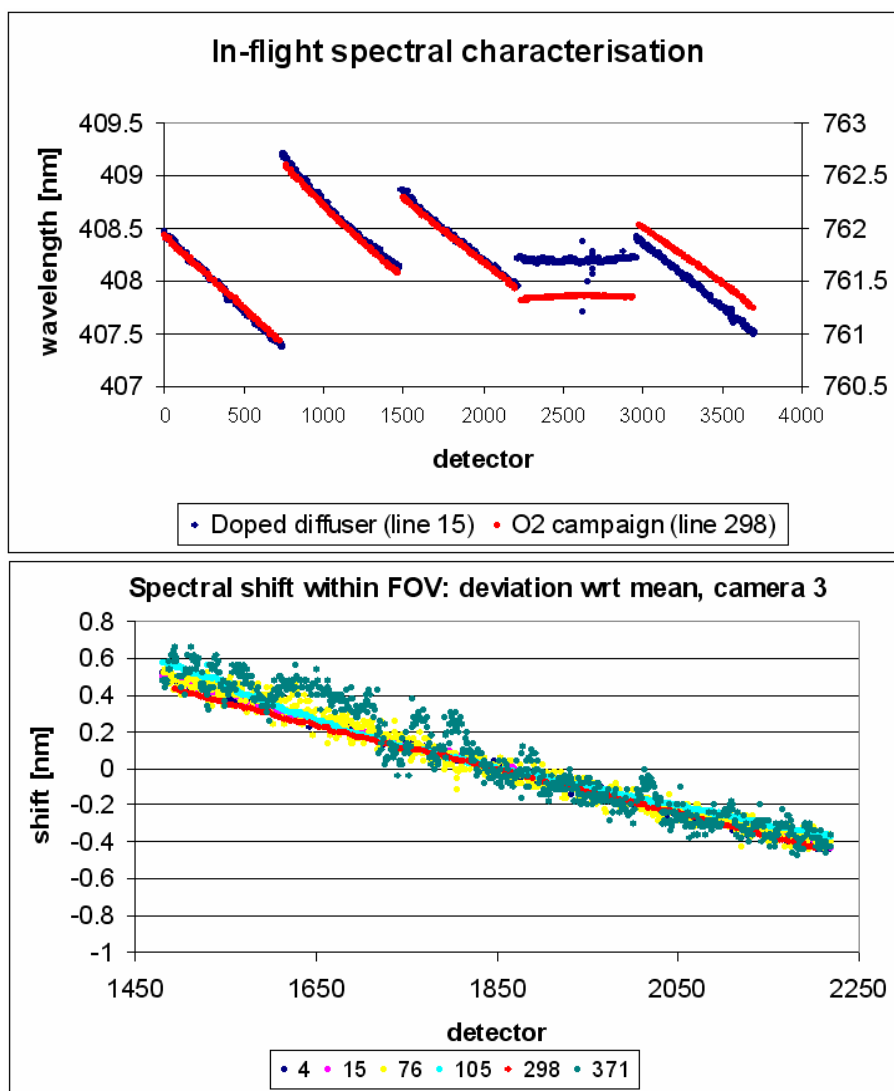


Figure 2: Top: Examples of in-flight spectral characterisation data highlighting the “smile effect”. Bottom: Spectral shift within the FOV of camera #3 according to characterisation data at several detector rows spread over the whole spectral domain.

The spectrometer’s “smile” has a fairly linear behaviour across the field of view of all cameras and this variation appears to be independent of the absolute wavelength. The intra-camera “smile effect” has been characterised at several wavelengths covering almost the whole spectral domain of the OLCI nominal channels. The whole data set is summarised on the figure below.

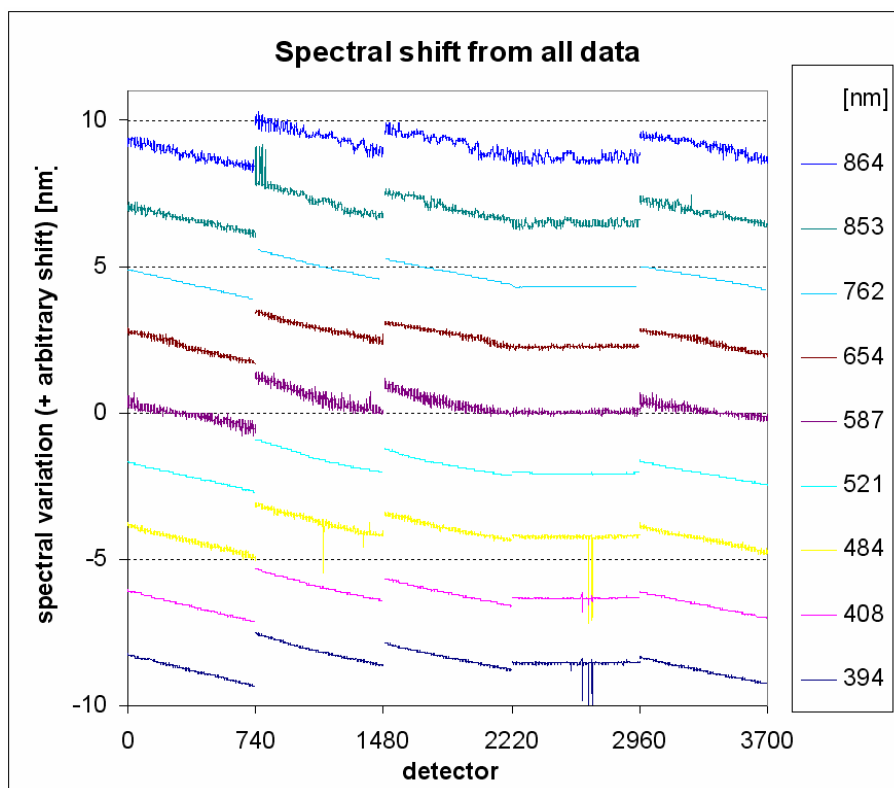


Figure 3: The “smile effect” at camera borders.

From these in-flight measurements, a spectral model was derived allowing to retrieve the central wavelength of every MERIS CCD cell. Unfortunately, no reliable method to characterised in flight the spectral width could be identified and the model had to rely on the sparse on-ground characterisation. It is out of the scope of the present document to present the MERIS spectral model in details but its essential characteristics are that a set of analytic function of CCD rows and columns allow retrieving the central wavelength and bandwidth for every CCD cell. There is one such set for each camera.

Examples of the outputs of the MERIS models are shown below for wavelengths, in-band irradiance, and normalised spectral response curves are shown on for a set of bands representative of the most common (10 and 7.5 nm) and extremes (3.75 and 20 nm) bandwidths of the MERIS nominal band set.

It should be noted that, according to its spectral model, MERIS does not comply with one of the OLCI spectral quality specification criteria listed above: the peak to peak variation is around 1.7 nm for all bands (while 1.4 is requested for OLCI).

On the other hand, the RMS is around 0.4 (1.0 requested) but one shall bear in mind that the modelling removes part of the variability.

Examples of normalised Spectral Response Curves are shown below, for a set of bands representative of the most common (10 and 7.5 nm) and extremes (3.75 and 20 nm) bandwidths of the MERIS nominal band set.

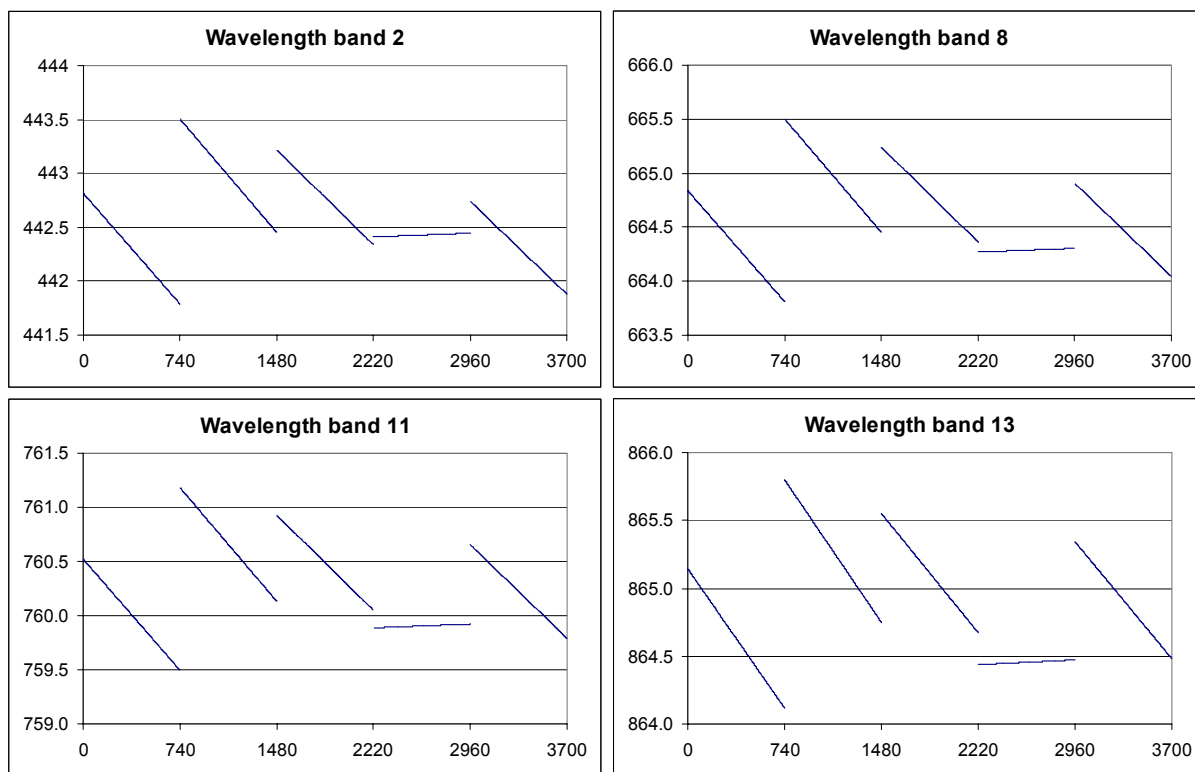


Figure 4: examples of in-FOV variation of wavelength for MERIS at 442, 665, 761 and 865 nm from top to bottom. Variations are white (independent of channel average wavelength) and reaches 1.7 nm peak to peak, and up to 1 nm within a given camera (from 0.4% and 0.25% resp. at 412 to 0.2% and 0.12% resp. at 865nm).

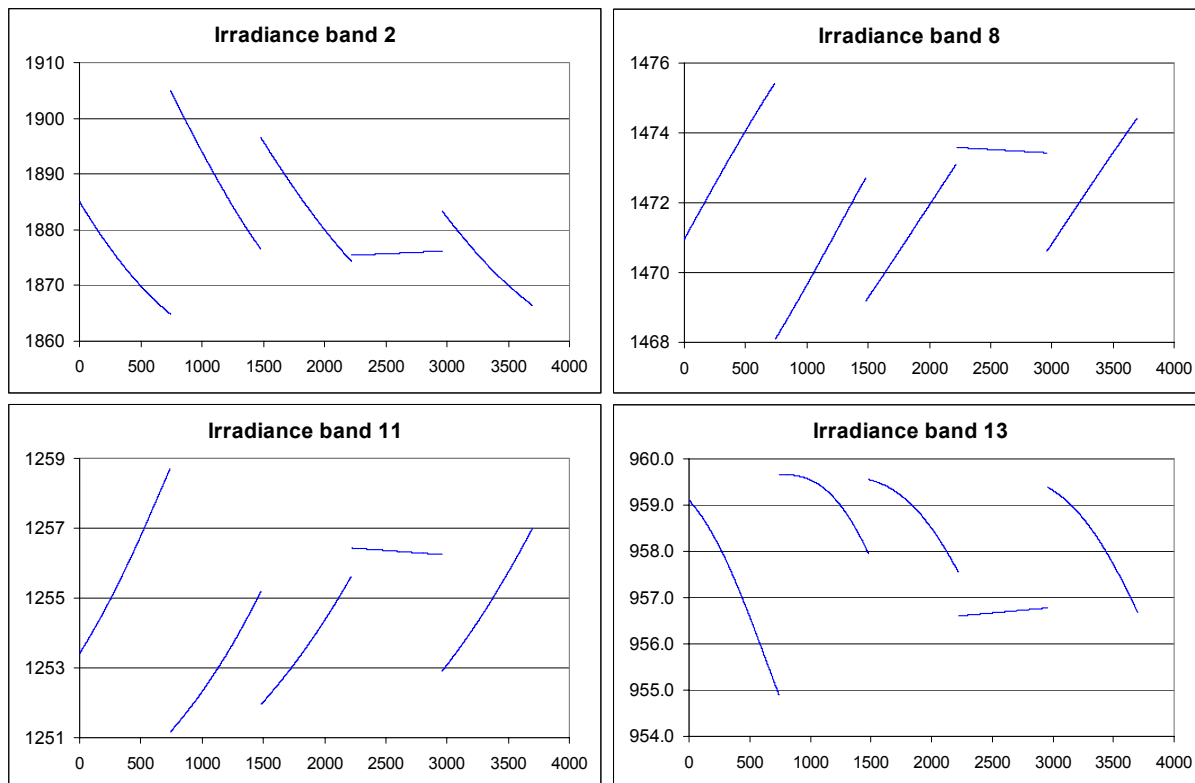


Figure 5: examples of in-FOV variation of in-band irradiance for MERIS at 442, 665, 761 and 865 nm from top to bottom. Variations can go from fairly stable (0.5% at 665nm) up to really significant (2.1% at 442).

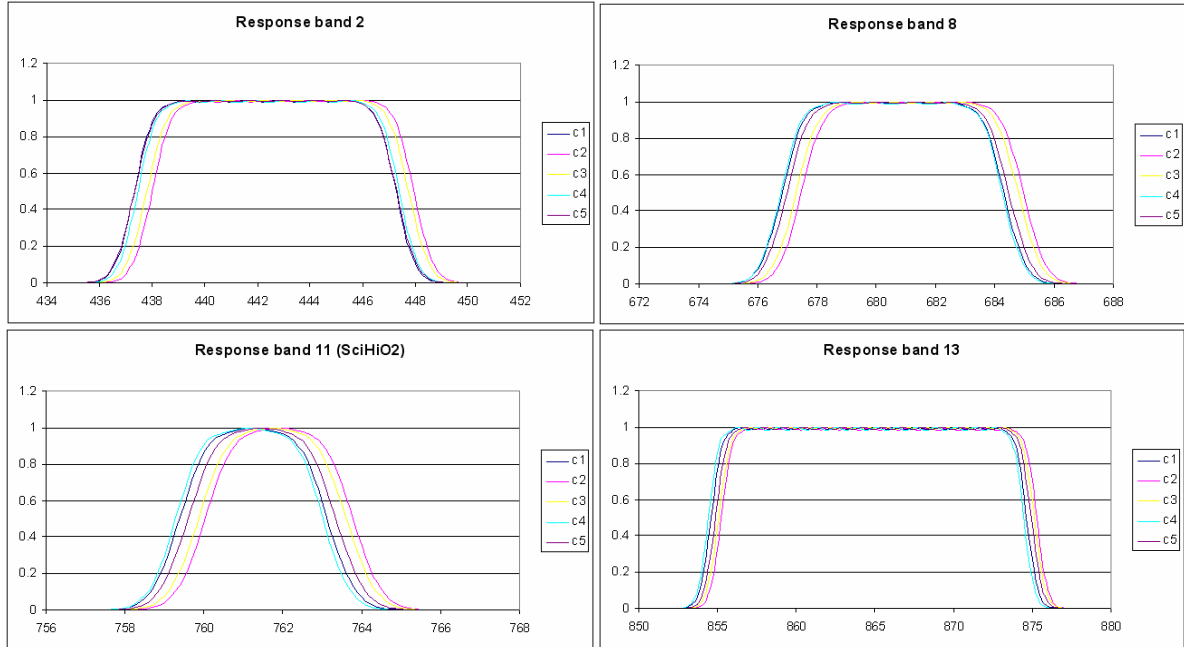


Figure 6: examples of MERIS bands normalised Spectral Response curves for typical (10 and 7.5 nm, top left and right) and extremes (3.75 and 20 nm, bottom left and right) bandwidths. Curves are given at camera FOV centre, and intra-camera spectral shift shall be added on top.



3. ALGORITHM DESCRIPTION

The Instrument Correction algorithm is split in two steps:

1. accurate TOA reflectance computation and
2. TOA reflectance correction

The first step is mandatory and removes most of the small scale radiance variations due to the non-constant central wavelength of a given band across the instrument field of view, at least for spectrally smooth targets. It shall be applied prior to any algorithm, even if they require radiance as input. In that case an additional backward conversion to radiance may be applied using solar flux values for nominal wavelengths and bandwidths.

The second step is proposed as an option. It shall apply only to clear sky pixels, with specific algorithms for water and land pixels.

Correction is not made on all bands but restricted to a predefined subset for which those variations can induce significant distortions when used in algorithms based on a fixed wavelength scheme. This subset of bands should ensure smoothness of reflectance local variations with wavelength and allow a good estimation of the reflectance derivative using neighbour bands. The selection of the neighbouring bands shall also be done carefully to ensure best possible spectral slope estimate. The algorithm, for each surface type, is thus parameterised by three band dependent parameters: the activation switch and the pair of bands from which the spectral slope is to be derived.

There are specific parameter sets for land and water surface types.

Table 2 presents a preliminary set of subsets for water and land in line with the bands definition of Table 1. It also provides the nominal in-band solar irradiance (at reference Sun-Earth distance) that may be used to convert reflectance output by either step 1 or step 2 back to radiance.

Those preliminary settings will have to be carefully revised on the basis of the downstream algorithms. This analysis should also establish whether the same scheme can be applied to all downstream algorithms of a given processing branch (water or land) or if correction setting shall be further split according to algorithms needs.



Table 2: Standard configuration of the reflectance correction.

| Band | Water | | | Land | | | Reference Central wavelength (nm) | E_0 ($W \cdot m^{-2} \cdot \mu m^{-1}$) |
|------|-------------------------------|------------|------------|-------------------------------|------------|------------|-----------------------------------|---|
| | reflectance correction switch | Lower band | Upper band | reflectance correction switch | Lower band | Upper band | | |
| O1 | 1 | O1 | O2 | 1 | O1 | O2 | 400 | 1,4418 |
| O2 | 1 | O1 | O3 | 1 | O1 | O3 | 412.5 | 1,6852 |
| O3 | 1 | O2 | O4 | 1 | O2 | O4 | 442.5 | 1,8641 |
| O4 | 1 | O3 | O5 | 1 | O3 | O5 | 490 | 1,9237 |
| O5 | 1 | O4 | O6 | 1 | O4 | O6 | 510 | 1,9435 |
| O6 | 1 | O5 | O7 | 1 | O5 | O7 | 560 | 1,8044 |
| O7 | 1 | O6 | O8 | 1 | O6 | O8 | 620 | 1,6534 |
| O8 | 1 | O7 | O9 | 1 | O7 | O9 | 665 | 1,5323 |
| O9 | 1 | O8 | O9 | 1 | O8 | O10 | 673.75 | 1,4979 |
| O10 | 0 | N/A | N/A | 1 | O9 | O11 | 681.25 | 1,4724 |
| O11 | 1 | O11 | O12 | 1 | O10 | O12 | 708.75 | 1,4084 |
| O12 | 1 | O11 | O12 | 1 | O11 | O12 | 753.75 | 1,2659 |
| O13 | 0 | N/A | N/A | 0 | N/A | N/A | 761.25 | 1,2521 |
| O14 | 0 | N/A | N/A | 0 | N/A | N/A | 764.375 | 1,2485 |
| O15 | 0 | N/A | N/A | 0 | N/A | N/A | 767.5 | 1,2221 |
| O16 | 1 | O16 | O17 | 1 | O16 | O17 | 778.75 | 1,1845 |
| O17 | 1 | O16 | O18 | 1 | O16 | O18 | 865 | 0,9582 |
| O18 | 1 | O17 | O18 | 1 | O17 | O18 | 885 | 0,9295 |
| O19 | 0 | N/A | N/A | 0 | N/A | N/A | 900 | 0,8957 |
| O20 | 0 | N/A | N/A | 0 | N/A | N/A | 940 | 0,8247 |
| O21 | 1 | O18 | O21 | 1 | O18 | O21 | 1020 | 0,6940 |

The reflectance correction switches define the bands on which it shall apply. The lower and upper band indices specify the adjacent bands to be used for spectral slope estimates. The reference wavelength is the wavelength to which reflectance is corrected, and E_0 the corresponding solar irradiance.

3.1 Theoretical Description

3.1.1 The radiance to reflectance conversion

Use of per pixel in-band equivalent irradiance in the conversion of radiance into top-of-atmosphere (TOA) reflectance:

$$\rho(\lambda_{b,pixel}) = \pi \cdot \frac{L(\lambda_{b,pixel})}{E_0(\lambda_{b,pixel}) \cdot \cos(\theta_s)} \quad \text{Eq. 1}$$



where L is the measured radiance at pixel wavelength, E_0 the in-band irradiance corrected for daily variations, and θ_S is the Sun zenith angle at the pixel location

It should be noted here that pixel specifically refers to an instrument (set of) detectors, and not to an image co-ordinate. Should the latter differ from the former, it is assumed that the Level 1 product provides a suitable way to establish a non ambiguous correspondence.

That correction is systematically applied to all 21 bands and requires the use of the same spectral model than the one used during Level 1 processing, in order to remain consistent with instrument calibration. It is assumed that a consistently computed set of solar flux values are provided by the Level 1, preferably within the Level 1 product itself to ensure optimised configuration control. It is assumed as well that the Sun zenith angles are available from the Level 1 product.

Apart from that it does not require particular applicability conditions or specific auxiliary data. Should any Level 2 algorithm require radiance as input, the can be derived thanks to:

$$L'(\lambda_{btheo}) \approx \frac{\rho(\lambda_{b,pixel}) \cdot E_0^{ref}(\lambda_{btheo}) \cdot \cos(\theta_S)}{\pi} \quad \text{Eq. 2}$$

Preliminary values of $E_0^{ref}(\lambda_{btheo})$ are given in Table 2

3.1.2 The reflectance correction

The reflectance correction, that is often referred to as the “smile correction”, consists in the correction of TOA reflectance from pixel wavelength to nominal one, using a first order Taylor expansion. **It applies to reflectances which are already corrected for gaseous absorption.** The rationale for that is twofold:

- ❖ Gaseous absorption often falls into the category of “sharp spectral signature” that the present algorithm is unable to handle accurately
- ❖ Some corrections schemes may perfectly handle variable wavelengths providing they are accurately known

3.1.2.1 Case of Land pixels

The main idea is the following, ie a first order Taylor approximation, assuming that the TOA reflectances, once corrected for gaseous absorption, are quite smooth wrt wavelength:

$$\rho_{corr}(\lambda_0) = \rho_{meas}(\lambda_{pixel}) + \frac{\partial \rho}{\partial \lambda} \cdot (\lambda_0 - \lambda_{pixel}) \quad \text{Eq. 3}$$

where the local reflectance spectral derivative is estimated by finite differences:

$$\frac{\partial \rho}{\partial \lambda} \approx \left[\frac{\rho_{meas}(\lambda_{2,pixel}) - \rho_{meas}(\lambda_{1,pixel})}{(\lambda_{2,pixel} - \lambda_{1,pixel})} \right] \quad \text{Eq. 4}$$

Note: based on the MERIS heritage, this processing should apply to the OTCI processing, but not to the OGVI one.

3.1.2.2 Case of water pixels

In the case of water pixels, the accuracy of the correction can be improved taking advantage of accurate knowledge of the Rayleigh scattering (LUTs). This is particularly relevant since Rayleigh scattering is generally by far the signal contributor with the highest spectral slope (in absolute). Over clear to moderately turbid waters, the coupling between molecular and aerosol scattering is sufficiently small to be considered as negligible in the frame of the reflectance correction. We thus propose a correction scheme that splits the signal into Rayleigh reflectance and Rayleigh corrected reflectance, accounting for the remaining contributors: water, water-air interface, aerosols and coupling terms.

Let's denote ρ_R the Rayleigh part and ρ_r the residue, so that we have: $\rho_{TOA} = \rho_R + \rho_r$. The strong spectral dependence of the molecular contribution is best captured if discrete derivatives of the logarithm of ρ_R (Figure 7) are used, instead of discrete derivatives of ρ_R , as shown in Figure 8 (red curve).

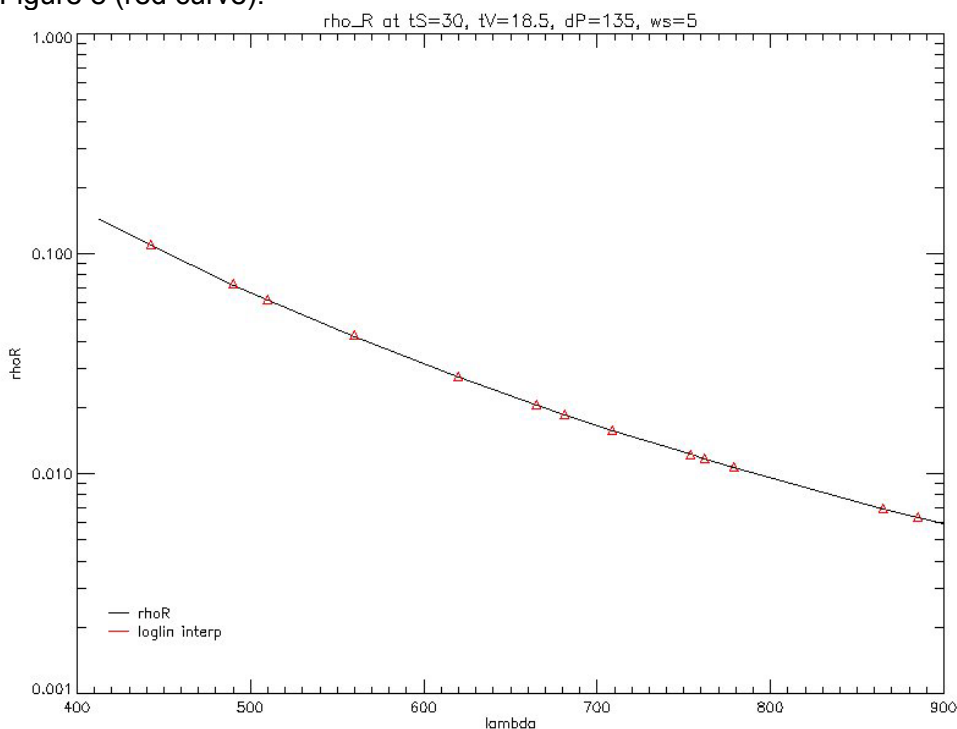


Figure 7: Logarithm of the Rayleigh reflectance at $\theta_s = 30^\circ$, $\theta_v = 18.5^\circ$, $\Delta\phi = 135^\circ$, $w = 5\text{m/s}$, as a function of wavelength.

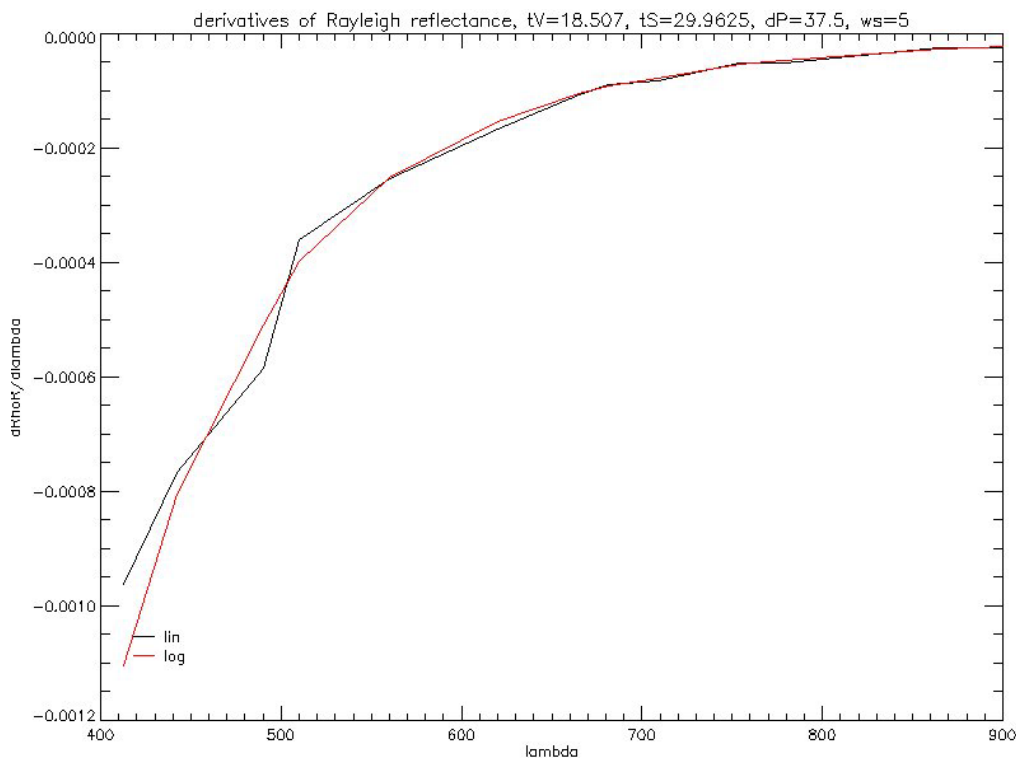


Figure 8: Derivatives of the Rayleigh reflectance computed with the Rayleigh reflectance versus the logarithm of the Rayleigh reflectance.

Presumably, the spectral dependence of the residue is less pronounced, at least outside of the red region, so that discrete derivatives taken on the residue may be acceptable.

Ignoring for the moment the specific problems posed by the chlorophyll absorption peak at 665 nm and the fluorescence band at 673 & 681 nm, the correction consists in:

- 1) extrapolating the Rayleigh contribution known at nominal wavelengths to the exact wavelength of a pixel,
- 2) subtracting this contribution to the TOA reflectance,
- 3) extrapolating residue from pixel wavelength to nominal wavelength (1st order Taylor),
- 4) adding the nominal Rayleigh contribution back to the corrected residue.

This scheme should provide a better accuracy than the global correction on TOA reflectance (as applied to the land pixels). Figure 9 and Figure 10 show a comparison of the different smile correction algorithms along a transect in the Ligurian Sea.



Figure 9: Mediterranean scene used to test the smile algorithms. The transect used for Figure 10 is East to West, north of Corsica.

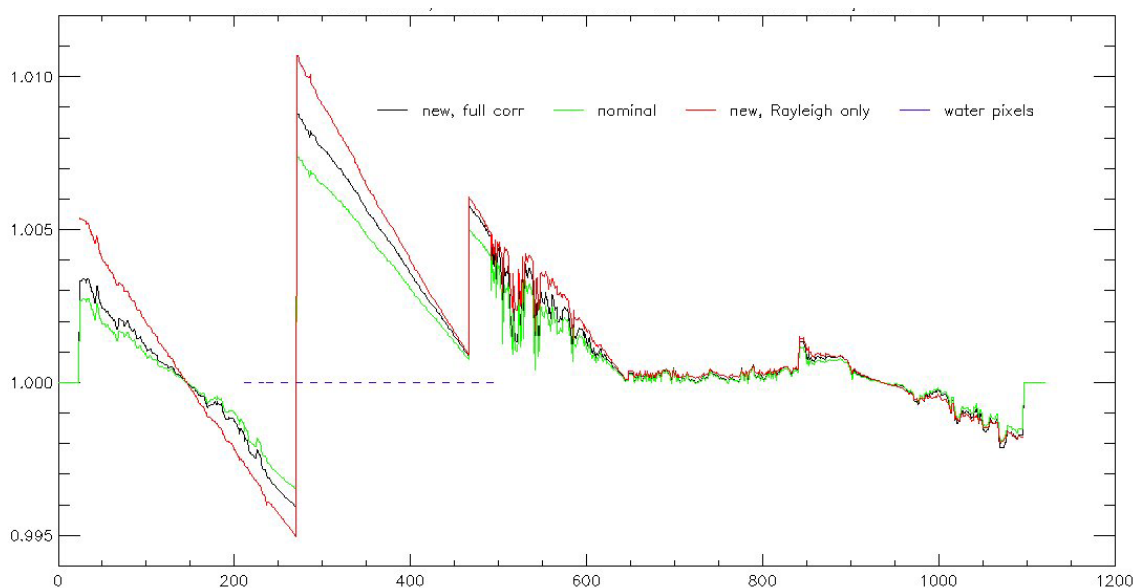


Figure 10: ratio of smile-corrected over non-corrected TOA reflectance in band 1 along a transect in the image in Figure 9.

Camera1 is to the left, camera 5 to the right. Current smile correction used for MERIS is represented in green (same as the proposed method for land pixels), smile correction limited to Rayleigh in red (steps 1, 2 & 4 of above algorithm description), and smile correction applied to both Rayleigh reflectance and residue in blue (steps 1 to 4). Water pixels are located in part of camera 1, camera 2 and a small part of camera 3 and identified by the horizontal dashed line.

Clearly, there exist large differences between these three smile corrections, the most accurate being presumably the double correction of the Rayleigh and the residue.



That step shall not be applied on every band: indeed, it requires to be carefully tuned to ensure that the local spectral variation around a given channel position can be estimated with sufficient accuracy by a linear approximation. If such conditions cannot be met, e.g. for bands located inside absorption lines like bands 12, 13, 19 and 23 or for sharp spectral features like phytoplankton chlorophyll fluorescence, the reflectance correction shall be disabled, thanks to the dedicated switches. For these reasons, the smile correction switches as well as the band pairs selected for the spectral slope estimates are specified according to the surface type below, namely water or land, via auxiliary data parameters. [Table 2](#) presents the setting of the operational Level 2 processing.

3.2 Algorithm Validation

This algorithm is satisfactorily used on MERIS data since early mission (the need had not been identified before launch), in an early version in which the method currently proposed for Land was applied also over Water. The version has proved to significantly improve the continuity at camera interface for sensitive products like TSM and YS (waters) or TCI (land). The evolution of the correction over water is part of the currently evaluated changes in the MERIS Level 2 processing chain, and no reported results are available yet. However it is based on theoretical considerations on the spectral shape of the Rayleigh scattering – confirmed by radiative transfer simulations – and it is thus expected to get better performances.

3.3 Practical Consideration

It is of utmost importance that the Smile Correction above water is applied using the same assumptions and auxiliary data regarding the Rayleigh scattering than the Atmosphere Correction algorithm, this to ensure full consistency of the output data with downstream processing.

The algorithm is designed to correct for small variations of the central wavelength of OLCI channels, using rough spectral slope estimates from nearby channels: it thus cannot correct for sharp spectral features like those induced by narrow atmospheric absorption lines or strong spectral transitions of relatively bright targets (e.g. the vegetation red-edge).

As a consequence it must be applied downstream an appropriate correction for gaseous absorption.



4. ASSUMPTIONS AND LIMITATIONS

The main assumptions of this algorithm are the following ones:

- 1) the smile effect is small in absolute values,
- 2) the spectral variation between cameras is in the order of 1.5 nm,
- 3) the variation inside cameras is in the order of 1nm.

However, the effect of such a variation is important, if the spectral bandwidth is small and/or if the slope of the measured spectrum is high. The largest impact of the smile effect is therefore in band O14, which is very narrow (3.75nm) and which is tentatively located in an absorption band. This band cannot be corrected by the procedure described above, and algorithms using this band, like pressure algorithms, have to use the exact wavelength per pixel.

It is assumed that this algorithm shall be applied after correction for residual gaseous absorption on those bands which are not dedicated to absorption measurements. Ideally, algorithms dedicated to gaseous absorption shall account for the in-FOV spectral variation.

The present algorithm is intended to provide a first order spectral correction of TOA signals of a smooth nature, in particular the scattering by atmospheric molecules and aerosols over targets that are either spectrally smooth.

It also should be noted that this strategy (the smile step) is not totally satisfying. A better way would be to directly account for the actual central wavelength for each product pixel in the geophysical algorithms, e.g. to derive the chlorophyll or the TSM.



5. AUXILIARY DATA

Two types of data are used for the instrumental correction: some are actually outputs from the level 1B, and the others are “auxiliary data”.

The outputs from the level 1B are the following:

- A vector of length 4865 (TBC) which gives the radiance for each product pixel and each band,
- A vector of length 4865 (TBC) which gives the detector index (instrumental pixel corresponding to the product pixel) (all the values in that vector are supposed to be integers in $[0, 5*740-1]$. “-1” means “no data”),
- The solar irradiance E_0 , already corrected for the day: it’s a matrix $21*(740*5)$, for the 21 bands and the 3700 instrumental pixels (the values in the table 2 are only there to be used potentially by an algorithm requiring radiances instead of reflectances),
- The central wavelength for each band and instrumental pixel: another matrix $21*(740*5)$.

The “auxiliary” data basically all appear in the table 2, and are all involved only in the smile step, that is to say, for both branches ocean and land:

- a vector of length 21 which gives the switches for the 1st order Taylor approximation (value is 0 or 1),
- a matrix $21*2$ which gives the 2 bands which are used to derive the slope (for each band), if the switch value is 1, N/A otherwise.
- **The Rayleigh reflectance above water look-up-table, from (or compatible with) the Atmosphere Correction above waters. The look-up-table shall span the 21 OLCI bands, the whole acquisition geometry domain (in terms of Sun and View zenith angle and relative azimuth angle) and the wind speed.**



6. ERROR BUDGET

An error model will be proposed on the basis of (at least):

- uncertainties on wavelengths and solar irradiance
- spectral deviation wrt reference wavelength of the corrected pixel
- local estimate of the spectral slope **from the available channels.**



7. REFERENCES

- [1] Delwart, S., R. Preusker, L. Bourg, R. Santer, D. Ramon and J. Fischer, 2005. MERIS in-flight spectral calibration, International Journal of Remote Sensing, MERIS Special Issue, Volume 28, Numbers 3 - 4, January 2007
- [2] S. Delwart, R. Preusker, L. Bourg, R. Santer, D. Ramon & J. Fischer, MERIS In-flight Spectral Calibration, Proceedings of the Second working meeting on MERIS and AATSR Calibration and Geophysical Validation, "MAVT-2006", available on-line at: http://envisat.esa.int/workshops/mavt_2006/papers/60_delwa.pdf
- [3] Thuillier, G., M. Hersé, D. Labs, T. Foujols, W. Peetermans, D. Gillotay, P. C. Simon, and H. Mandel, 2003, "The solar spectral irradiance from 200 to 2400 nm as measured by the SOLSPEC spectrometer from the ATLAS and EURECA missions", Sol. Phys., **214**: 1-22.
- [4] . Santer, R, F. Zagolski and E. Diligeard, " Radiative Transfer Code Comparison for Meris Vicarious Calibration" Proceedings of the Envisat Validation Workshop, 2002, (http://envisat.esa.int/workshops/validation_12_02/proceedings/meris/04_santer.pdf)